Journal of
Synchrotron
Radiation

ISSN 1600-5775

Received 27 August 2013
Accepted 25 June 2014

Biological soft X-ray tomography on beamline 2.1 at the Advanced Light Source

Mark A. Le Gros,[a,b,c]* Gerry McDermott,[a,b] Bertrand P. Cinquin,[a,b] Elizabeth A. Smith,[a,b] Myan Do,[a,b] Weilun L. Chao,[d] Patrick P. Naulleau[d] and Carolyn A. Larabell[a,b,c]*

[a]Department of Anatomy, School of Medicine, University of California San Francisco, San Francisco, CA 94143, USA, [b]National Center for X-ray Tomography, Advanced Light Source, Berkeley, CA 94720, USA, [c]Physical Biosciences Division, Lawrence Berkeley National Laboratory, Berkeley, CA 94720, USA, and [d]Center for X-ray Optics, Lawrence Berkeley National Laboratory, Berkeley, CA 94720, USA. *E-mail: mark.legros@ucsf.edu, carolyn.larabell@ucsf.edu

Beamline 2.1 (XM-2) is a transmission soft X-ray microscope in sector 2 of the Advanced Light Source at Lawrence Berkeley National Laboratory. XM-2 was designed, built and is now operated by the National Center for X-ray Tomography as a National Institutes of Health Biomedical Technology Research Resource. XM-2 is equipped with a cryogenic rotation stage to enable tomographic data collection from cryo-preserved cells, including large mammalian cells. During data collection the specimen is illuminated with 'water window' X-rays (284–543 eV). Illuminating photons are attenuated an order of magnitude more strongly by biomolecules than by water. Consequently, differences in molecular composition generate quantitative contrast in images of the specimen. Soft X-ray tomography is an information-rich three-dimensional imaging method that can be applied either as a standalone technique or as a component modality in correlative imaging studies.

Keywords: cell biology; cellular imaging; cryo-preservation; cryogenic fluorescence tomography; cryostage; three-dimensional reconstruction.

1. Introduction

Beamline 2.1 is a soft X-ray transmission microscope located in sector 2 of the Advanced Light Source (ALS) at Lawrence Berkeley National Laboratory. More commonly known as XM-2, this microscope was designed, constructed and is now operated by staff of the National Center for X-ray Tomography (NCXT; http://ncxt.lbl.gov). XM-2 is fully dedicated to biological imaging, in particular visualizing and quantifying cellular and sub-cellular organization using tomographic approaches. Unlike other high-spatial-resolution cellular imaging techniques such as electron tomography, soft X-ray tomography (SXT) has the capacity to image intact cells, including large mammalian cells (Weiss *et al.*, 2000, 2001; Schneider *et al.*, 2010, 2012; Larabell & Le Gros, 2004; Larabell & Nugent, 2010; Le Gros *et al.*, 2005; Sakdinawat & Attwood, 2010). As with all biological-imaging techniques, specimen illumination accumulated during SXT data acquisition has the potential to damage fine-structural details in the cell (Larabell & Nugent, 2010). Consequently, the specimen is cryo-preserved prior to SXT data collection to minimize radiation damage. Not only does cryo-preservation reduce structural damage to a level unseen in SXT images, it also fixes molecules and cellular structures in place during data acquisition. Specimens are typically mounted in thin-walled glass capillaries and flash-cooled prior to imaging in XM-2. A custom-designed cryogenic rotation stage (cryo-stage) enables collection of projection images from any arbitrary angle around a 360° central rotation axis (Parkinson *et al.*, 2013). In SXT, as with any tomographic imaging technique, systematically missing data (due to restricted rotation of the specimen) results in anisotropic spatial resolution and negatively impacts the overall quality of the tomographic reconstruction by adding artifacts, such as streaking (Hummel *et al.*, 2012; Hagen *et al.*, 2012; Parkinson *et al.*, 2013; Cardone *et al.*, 2005).

The primary users of XM-2 are cell biologists, often with little to no prior experience of working at a synchrotron. Consequently, human–instrument interfaces, such as the specimen-mounting system and the microscope control GUI, have been developed to hide the complexities of these systems from inexperienced users and incorporate features that enhance productivity, such as automated data analysis software package *AREC3D* (Parkinson *et al.*, 2012). Below we present an overview of beamline 2.1, and briefly describe some of the other technologies and resources available to users of the NCXT.

2. Beamline overview

An overview of the XM-2 instrumental layout is shown in Figs. 1(*a*) and 1(*b*), and the operating parameters are summarized in Table 1. The complete beamline, from the bending-magnet source to the CCD detector, is 19.71 m long. Currently the microscope can operate between 400 and 1300 eV. To date, all experimental data have been collected on XM-2 using 'water window' illumination (284–543 eV); however, in the future it is conceivable that data collection at higher energies may be desirable. To accommodate higher-energy modes of operation, all microscope components from the mirror chamber

Table 1
XM-2 operating parameters.

Beamline name	ALS beamline 2.1 (XM-2)
Source type	Bend magnet
Mirrors	Flat silicon; striped with nickel and gold surfaces
Monochromator	Zone-plate linear
Energy range (eV)	400–1300
Flux (512 eV)	5×10^7 photons s^{-1} μm^{-2}
Field of view	15 × 15 μm single field; capacity to tile unlimited fields of view
Rotation stage	Custom-designed cryo-rotation stage, allows specimen to be rotated through 360°
Specimen environment	70 K helium gas; specimen held at atmospheric pressure
Detector type	2048 × 2048 back-thinned CCD; pixel size 13.5 × 13.5 μm
Detector model	Andor iKon-L

downstream to the CCD detector are mounted on plates supported by air pads. When activated, the pads levitate the entire beamline on a frictionless cushion of air. Consequently, the entrance and exit angles of the X-ray source can be adjusted easily from 0.5° to 3° with respect to the mirror surface (Fig. 1*b*). This adjustability allows the operational energy range of the microscope to be extended up to 4 keV. Achieving this operational mode only requires simple upgrades to the radiation shielding, rather than requiring a major beamline redesign. This upgrade will be implemented once there is sufficient demand and scientific justification.

The optical set-up of XM-2 is that of a classical two-lens bright-field light microscope, and uses Fresnel zone plates as both condenser and objective lenses (Attwood, 1999; Kirz *et al.*, 1995; Falcone *et al.*, 2011). The flat mirror acts as a cut-off filter for high-energy photons. The condenser lens creates a 40× demagnified image of the X-ray source in the specimen region. The objective lens transmits a magnified image of the illuminated specimen onto the CCD detector. In combination with a central beam stop and a pinhole in close vicinity to the specimen, the condenser zone plate (as a diffractive element) acts as a linear zone plate monochromator (Attwood, 1999).

To have flexibility in the lens design and to make use of the energy range provided by the mirror, the optics holder in the condenser chamber was designed to have 1.4 m of free travel along the optical axis. Up to four condenser lenses can be mounted in the condenser holder, in two pairs along the optical axis. This configuration allows, for example, lenses with different spatial resolutions to be used sequentially to image the specimen. Three zone-plate objective lenses can be installed in parallel in the objective holder. A back-illuminated 2048 × 2048 pixel CCD from Andor, with a pixel size of 13.5 μm, is used as the detector.

We will now describe the microscope in more detail, beginning with the X-ray source.

2.1. Low-field bend-magnet X-ray source

A low field (1.3 T) bend-magnet source at the ALS is ideal for soft X-ray microscopy as the peak brightness occurs over the important 'water window' wavelength range. The ALS storage ring operates at 1.9 GeV and a constant beam current of 500 mA. The source is sufficiently stable that flat-field images are acquired only at the start and end of each tomographic data set, rather than after each individual projection image. At bend magnet 2.1, a recent upgrade to the ALS lattice resulted in the electron beam being 32.7 μm wide and 32.6 μm high. It is a line source with the vertical divergence controlled largely by the synchrotron cone from 1.9 GeV electrons traversing a 1.3 T bend magnet. At a source-to-condenser distance of 18.2 m, a 1 cm-diameter condenser zone plate is optimally filled with 'water window' photons in the vertical direction and captures 0.5 mrad of the horizontal line source. The source is de-magnified 40 times onto the image plane and the modest optical performance of the condenser lens produces a 1 μm × 1 μm spot. The condenser is scanned using a precision XY scanner stage to produce a flat-field illumination pattern that fully utilizes the dynamic range of the detector when imaging cylindrical specimens. Since the condenser aperture is highly overfilled, the specimen illumination remains stable over time. Optimizing the alignment of XM-2 is straightforward, and has proven robust to source relocations due to synchrotron upgrades and seismic disturbances. This factor has contributed significantly to

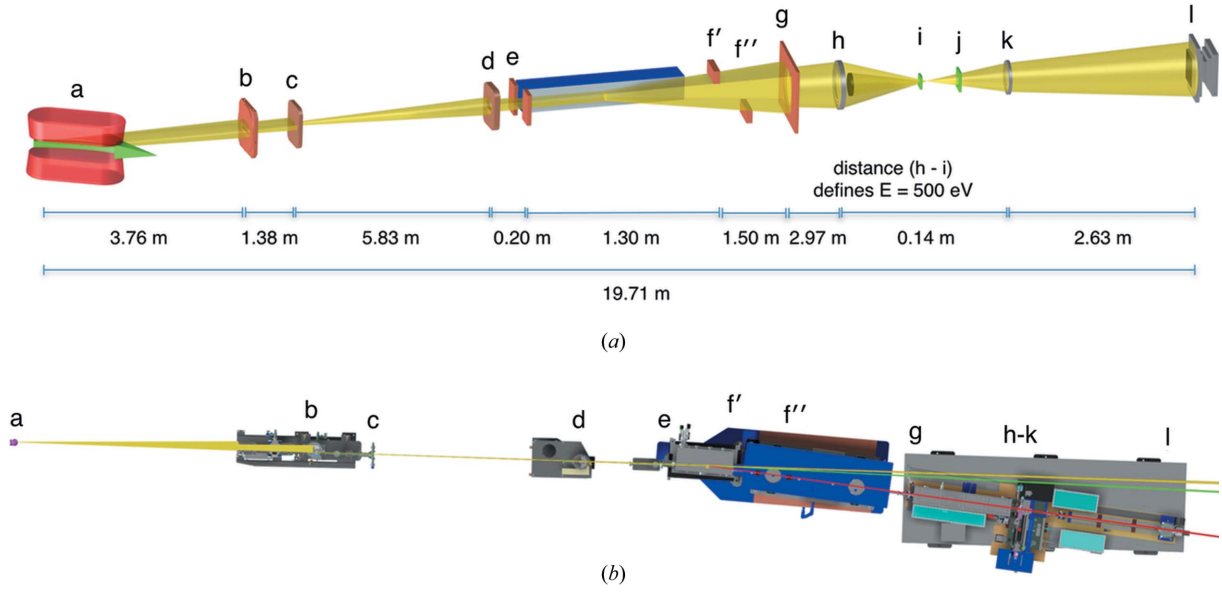

Figure 1
(*a*) Schematic of the optical layout of the soft X-ray microscope beamline XM-2. (a) Bend magnet (in red) and radiation source (green arrow); (b) water-cooled aperture; (c) branchline aperture; (d) mirror box front aperture; (e) mirror horizontal slits; (f′) upper vertical slit; (f″) lower vertical slit; (g) condenser aperture; (h) condenser zone plate lens; (i) condenser chamber vacuum window and monochrometer pinhole; (j) MZP chamber vacuum window; (k) micro zone plate (objective lens); (l) camera. The mirror is shown in blue and located between (e) and (f′). Figure not drawn to scale. (*b*) Schematic of the optical layout of XM-2. (a) Source; (b) water-cooled aperture; (c) branchline aperture; (d) mirror box front aperture; (e) mirror horizontal slits; (f′) upper vertical slit; (f″) lower vertical slits; (g) condenser aperture; (h)–(k) condenser zone plate lens, front pinhole, specimen plane, micro zone plate (objective lens); (l) camera. Figure not drawn to scale. X-ray light path color code: yellow, 0°; green, 1°; red, 3°.

the large number of whole cell tomograms generated by users of the facility.

2.2. Front-end assembly

The 'front-end' assembly interfaces the end-station with the storage ring. The front-end consists of a number of ultra-high-vacuum fast valves interlocked to pressure sensors along the beamline. The fast valves rapidly isolate the storage ring in the event of an accidental vacuum breach further along the beamline. The front-end also contains a number of fast water-cooled photon stops, apertures and radiation shields.

2.3. Branchline

The ALS bend magnet that provides illumination to beamline 2.1 produces a beam with a horizontal swath of 200 mrad and a vertical emittance of the order of 3 mrad for X-rays at energies appropriate for soft X-ray microscopy. A beam-defining aperture in the front-end generates a beam of 2 mrad in both the horizontal and vertical direction. The total power generated from the bend magnet source is 3 kW into the full 200 mrad horizontal emission pattern. After collimation by the front-end apertures, the total power leaving the concrete shielding of the storage ring is $\sim$30 W. The spectrum of radiation allowed into the beamline extends from the infrared range up to the energy of the stored electrons, in this case 1.9 GeV. The very high energy photons are generated from bremsstrahlung processes due to electrons in the storage ring interacting with residual gas molecules in the storage ring vacuum chamber. This results in a spectrum of gas bremsstrahlung photons with a peak flux at approximately 10 MeV. The beamline 2.1 branchline modifies the spectrum of the radiation and controls the beam direction. The branchline also stops high-energy bremsstrahlung radiation by using a 30 cm cube of lead in line with a direct path to the source. A flat X-ray mirror deflects bend-magnet radiation and the spectrum of deflected X-rays depends on the grazing angle of the mirror and the coating used. For a 3° grazing angle and a nickel coating, X-rays above 700 eV are strongly attenuated; therefore this choice of angle and coating is most suitable for water window imaging. Another function of the branchline is to provide an additional level of vacuum protection for the storage ring *via* a fast shut-off valve.

2.4. X-ray mirror

The X-ray mirror is located just outside of the ALS shield wall. This optic redirects X-rays with the desired spectral range to the condenser system of the microscope. In addition to this filtering action, the mirror is also fully motorized to allow alignment of the illumination beam with the optical axes of the microscope end-station. The mirror is a flat optic with a measured tangential slope error of 1.14 µrad r.m.s. over 700 mm, corresponding to 67 km radius of curvature; and a sagittal slope error of 7.85 µrad r.m.s. over 40 mm, corresponding to 33.38 km radius of curvature. The surface roughness was 2.5 Å r.m.s. We selected a silicon substrate 700 mm in length and 40 mm wide with two reflective stripes: one nickel and the other gold. The extra gold coating was chosen to enable the microscope to operate at energies not reflected by the nickel mirror, in particular energies close to nickel X-ray absorption edges. The mirror (SESO Inc., France) is water-cooled *via* a nickel-coated cold finger immersed in a liquid-gallium contact bath. The complete mirror box assembly is a UHV vacuum system held at low pressure by a 500 l s^{-1} ion pump. The mirror box, associated motorization and LabView (http://www.ni.com) control system was provided by Oxford Danfysik (http://www.oxford-danfysik.com) according to specifications from NCXT staff.

2.5. Delay line

This section of the branchline is a simple but necessary part of the vacuum isolation system. To exploit the wide divergence angle of a bend-magnet X-ray source, and to keep the first mirror a simple planar optic, it is necessary to place the X-ray microscope close to the storage ring. Therefore, a vacuum delay line is required for storage-ring vacuum protection. The delay line consists of two large vacuum tanks connected by a relatively low pumping conductance tube. Each vacuum vessel is independently pumped. The chamber closest to the storage ring is connected to an ion pump. A turbo pump maintains vacuum in the other chamber. There are also vacuum isolation valves between the chambers, as well as a high-speed fast valve that acts to quickly isolate the mirror chamber during a vacuum failure. Such a failure could result from the rupture of one of the thin 100 nm-thick silicon nitride windows in the downstream components of the X-ray microscope. The large volume of the delay line chambers would attenuate such a pressure spike, slowing the pressure rise in the ultra-high-vacuum regions of the beamline. This would allow time for the fast valve mechanisms to close and prevents the pressure in the mirror box from rising to a level too high for the mirror box ion pump. All valves are controlled by a computerized protection system called the 'Equipment Protection System', otherwise known as EPS.

2.6. X-ray illumination system (KZP box)

The X-ray illumination system is analogous to the condenser system used in bright-field visible-light microscopy. It focuses the source radiation onto the specimen, optimally matching the numerical aperture of the specimen illumination to that of the objective micro zone plate lens. The condenser zone plate (known as KZP to conform to the original German nomenclature) has 41667 zones made with approximately 200 nm-thick nickel. The diameter of the optic is 1 cm with a 5 mm central stop. The condenser zone plate lens also functions as an X-ray monochromator. The bend-magnet source radiation is broadband, but transmission X-ray microscopy requires narrow-band illumination due to strong chromatic effects in zone-plate imaging. To circumvent this problem, the condenser is configured as a linear monochromator, formed by the condenser zone plate and a pinhole placed close to the specimen (Hirai *et al.*, 1999). The relative bandwidth of this monochromator is determined by the width of the condenser zone plate lens, the size of the pinhole and the source demagnification factor; $(E/\Delta E)$ has a value of 300 for the lens and pinholes typically used. The focal length of a Fresnel zone plate lens is inversely proportional to the wavelength focused. Consequently, moving the condenser zone plate relative to the pinhole can vary the photon energy used to illuminate the specimen.

The total condenser zone plate travel is 1600 mm, with a minimum condenser to specimen distance of 37 mm. The corresponding imaging wavelength therefore varies in the range 1 nm $\leq \lambda \leq$ 13 nm. Both the condenser and the condenser pinhole are mounted on a three-axis computer-controlled stage to allow alignment of all components to a common optical axis.

The bend-magnet X-ray source is imaged through the monochromator pinhole and onto the specimen by the condenser zone plate. This type of illumination is referred to as critical illumination. The spot size of the imaged source at the specimen is less than 2 µm in diameter; as a result, it is necessary to scan the condenser in order to uniformly illuminate the desired field of view. The field of view for beamline 2.1 is 15 µm $\times$ 15 µm. The condenser is mounted on a

precision-encoded piezoelectric flexure stage and the scanning pattern is adjustable and synchronized with image acquisition on the CCD. The stage can accommodate multiple condenser lenses to allow optimization of zone-plate lifetime. As one condenser degrades due to radiation damage, a new condenser can be mounted, allowing the old condenser to be used for alignment and non-critical imaging procedures. The condenser is monitored for signs of degradation by observing the size and shape of the reimaged source, and recording a spectral image of a standard titanium oxide specimen. That said, minimal degradation of condenser performance has been observed over time. KZP optics that have been in heavy use for the past four years are still capable of high-quality imaging.

When the 'best quality' image is required, the high performance condenser is moved into position for imaging. All stages in the condenser box are indexed and position-encoded to a resolution better than 100 nm to enable simple set-up and alignment prior to each imaging session. The condenser vacuum box is pumped by a turbo-molecular pump as well as a liquid-nitrogen-cooled cryo-trap. The cryo-trap ensures a clean vacuum, which helps to prevent X-ray induced contamination build-up on the X-ray optics. Once the KZP chamber has been pumped to a low pressure, the turbo-molecular pump can be switched off and maintained at low pressure by a cryo-trap and vacuum pumps in the branchline. This helps stop vibration from being transferred to the cryo-rotation stage, which could lead to degradation of the X-ray image. A neutral density filter wheel, at the entry of the KZP box, can be used to fine-tune the acquisition protocol and avoid over-exposure or saturation of the CCD detector during binned video mode operation. This mode enables automation of the specimen alignment procedures without the introduction of excessive radiation damage.

2.7. X-ray image formation system (MZP box)

The micro zone plate (MZP) function is analogous to the objective lens in bright-field light microscopy. Namely, it gathers transmitted light from the specimen and focuses a magnified imaged of the specimen onto the CCD detector. The MZP is housed in a vacuum enclosure containing two precision encoded three-axis (X, Y, Z) stages. One stage controls the position of the MZP; the other stage positions a phase ring in the MZP's back focal plane. As the energy or magnification used for imaging varies, both the MZP and phase plate need to be adjusted relative to the specimen. For direct absorption imaging the phase plate is moved out of the beam path completely. This is the only fully operational mode of imaging for synchrotron users at the present time.

The vacuum requirements in this part of the microscope are not as strict as those for the KZP box and other parts of the instrument closer to the storage ring. However, it is important to ensure a low hydrocarbon environment to prevent X-ray-induced polymerization of organic compounds on the zone plate optic or other sites of high X-ray flux, such as the thin window on the vacuum isolation cone. The microscope can accommodate two or more objective lenses, allowing multi-resolution imaging of a specimen. The MZP support arm is attached to a kinematic base and thus enables the whole structure to be easily removed through the vacuum hatch at the top of the MZP box. To accommodate different imaging conditions, such as resolution, working distance, field of view and depth of field (DOF), several designs of MZPs were fabricated using electron beam lithography. The MZPs are all made with nickel zones and have a diameter in the region of 70 µm. The higher-resolution MZP has an outer zone width of 50 nm, a focal length of 1.5 mm and a DOF of ± 2 µm at a wavelength of 2.4 nm. The larger DOF MZPs have an outer zone width of 80 nm, a focal length of 2.4 mm and a DOF of ± 5 µm at 2.4 nm wavelength. These zone-plate parameters were chosen to maximize the types of specimen than can be imaged by SXT. A planned future development is to increase the imaging resolution on XM-2. In two-dimensional imaging, state-of-the-art zone plates have demonstrated to deliver spatial resolution in the regime of 10 nm (Chao *et al.*, 2012; Vila-Comamala *et al.*, 2009; Rehbein *et al.*, 2012). Since the DOF decreases quadratically with resolution, using high-resolution MZP optics will require techniques such as deconvolution to be applied when imaging specimens thicker than the DOF. Alternatively, use of non-conventional optics, such as cubic zone plates, could potentially increase the resolution without such a significant decrease in DOF.

2.8. Detector

The detector of choice for soft X-ray imaging is currently a back-thinned cooled CCD. The CCD camera on beamline 2.1 was manufactured by ANDOR instruments (http://www.andor.com) model iKon-L DO936N BN9KH. The camera has 2048 × 2048 pixels, each of which is 13.5 µm × 13.5 µm. The CCD is back-illuminated with no anti-reflection coating and has a 16-bit, 1 MHz readout analog-to-digital converter (ADC) and 14-bit, 3–5 MHz readout capability. The CCD chip in this camera is manufactured by E2V Inc. (http://www.e2v.com), and is cooled to 243 K by a Peltier cooling stack. As the microscope magnification is changed, the camera needs to move along the optical bench; it has a total range of motion of 200 cm. In addition to direct cooling of the CCD to reduce dark-current noise, a liquid-nitrogen-cooled water trap is connected to the CCD vacuum system. This ensures that any moisture present in the vacuum system preferentially condenses and freezes in the cold trap rather than on the surface of the CCD. A fast shut-off valve is also placed just in front of the camera; this valve activates in the event of a rupture of the thin MZP window, again protecting the detector from atmospheric moisture.

2.9. Cryogenic specimen rotation stage for tomographic data acquisition

NCXT staff designed and constructed a cryogenic specimen stage (cryo-stage) that can be used for single-axis tomographic measurements on both flat and cylindrical specimens. For specimens loaded into thin-wall glass capillaries, acquisition of tomographic data sets that take advantage of 360° of rotation is typical. For extended flat specimens full rotation is not possible due to both the mechanical interference between the specimen and microscope components (Fig. 2*a*) and the thickness of a flat specimen increasing as a function of increasing tilt. The system is designed to allow up to ±75° tomography on such flat specimens. Rotation of the specimen is provided around an axis defined by two high-precision spheres in the rotation stage. A tip/tilt eucentric correction stage rotates with the specimen to bring the region of interest onto the rotation axis (Fig. 2*b*).

The cryo-stage is based on many of the ideas and techniques commonly used in macromolecular crystallography. The specimen is mounted on an X, Y, Z, θ stage, and an encoded motorized stage is used to center the region of interest in the specimen on the rotation axis. A two-axis picomotor-actuated stage is positioned above the specimen tube and rotates with the specimen. Centering for specimens mounted in capillaries is first performed using a light microscope to ensure no more than a 1 µm deviation as the specimen is rotated through 180°. Further improvement in alignment is performed using a sequence of four low-dose X-ray images to first view and then position the rotation axis to better than 0.25 µm. The first alignment image is taken at 0° rotation and the position of the

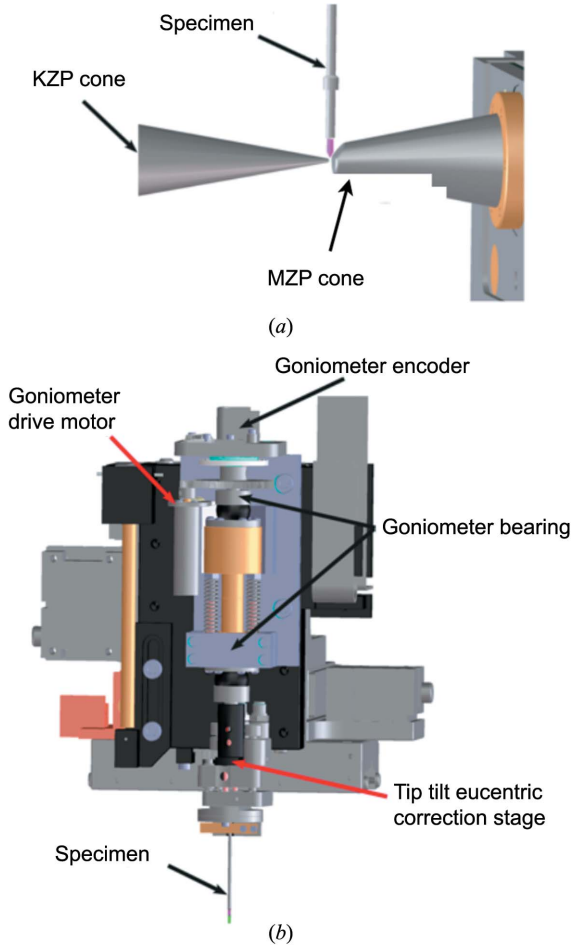

Figure 2
(*a*) Close-up view of the specimen environment relative to the two zone plate cones. The specimen mounted in a thin-walled glass capillary is shown in pink [KZP = condenser zone plate; MZP = micro (objective) zone plate]. (*b*) Details of the specimen rotation stage, showing the relative position of the major components.

specimen center is recorded. The specimen is then rotated to 180°, the new position is noted, and then the axial alignment stage is used to position the specimen at the mid-point of the 0°/180° specimen positions. The same procedure is used again for the 90°/270° specimen positions. After this procedure the specimen is well aligned to the rotation axis of the cryo-stage, and a complete tomographic data set can be collected without any refocusing of the specimen. The entire alignment procedure takes less than 20 s and is now being automated. The capillary tubes are of sufficiently high symmetry that 50–100 μm of the tube length is suitable for acquisition of a tomographic projection series after a single axial alignment.

The XM-2 cryo-stage is built around a Dewar filled with liquid nitrogen which provides a cold supply of nitrogen and helium gas. These gases are used to keep the specimen area and the specimen itself at cryogenic temperature. The specimen area is located in an insulated arm extending from the Dewar. A system of heat exchangers and heat shields is used to guarantee efficient cooling and shielding of the specimen.

The specimen is maintained at low temperature and atmospheric pressure by a stream of liquid-nitrogen-cooled helium gas. To ensure that the minimum flow of gas is used to maintain an adequately low temperature, we used a conduction-cooled intermediate heat shield. This heat shield provides most of the cooling power required to keep components that are close to the specimen cold, including items such as the KZP and MZP cones. The slow flow of cold helium gas also prevents the ingress of moisture. In Fig. 3 we show a simplified diagram of the cryogenic gas flow used to maintain the specimen at low temperature.

The intermediate heat shield is maintained at 90 K by thermal connection to a nitrogen gas primary cooling loop. The primary loop also cools a dual heat exchanger system that generates the low-temperature helium gas used for direct specimen cooling. This arrangement greatly reduces the flow of helium gas required to keep the specimen cold. The use of a low flow rate for final stage specimen cooling reduces the volume of helium gas exhausted to the atmosphere and helps prevent ice build-up and generation of local thermal gradients that cause the specimen to drift during image acquisition.

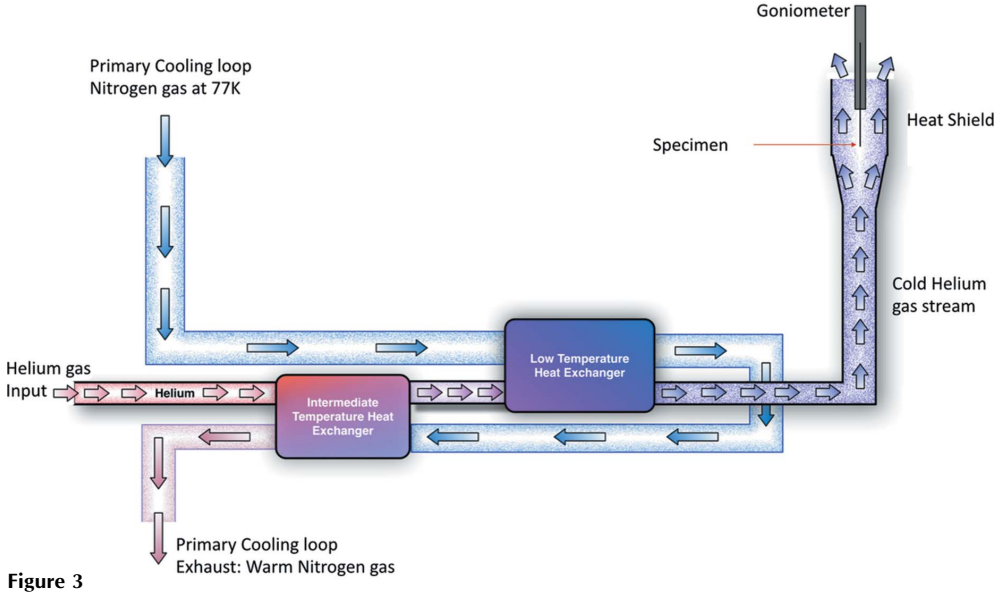

Figure 3
Gas flow in the cryo-stage cooling system. Helium cryogen gas first passes through an intermediate-temperature heat exchanger where it is cooled to ∼120 K, before passing through a low-temperature exchanger where it is further cooled to the desired specimen temperature. The 77 K nitrogen-cooling loop is shown relative to the helium gas flow and the two heat exchangers.

Specimen stability is a crucial part of high-resolution X-ray imaging. For a single high-spatial-resolution TXM image using a synchrotron source, one has to expect an exposure time of the order of 100 ms. This time scale is long enough for deterioration of the image quality by movement of an unfixed biological specimen in an aqueous environment and by radiation-induced damage. Tomographic investigations at a cellular level therefore require sufficient fixation procedures. Cryopreservation has been shown to be an excellent approach, allowing the collection of hundreds of high-resolution X-ray images of biological specimens without radiation damage being apparent in TXM images of the specimen.

Other than keeping the specimen at constant temperature, the cryogenic specimen stage has to provide a means of loading vitrified speci-

mens or, alternatively, freezing unfixed specimens directly at the instrument. Additionally, the stage has to position the specimen holder in the small air gap between the two vacuum windows of the condenser and objective chamber. Precise rotation of the object around an axis going through a user-defined region of an extended specimen has to be provided for automatic tomographic data capturing procedures. Means of inspecting and aligning a region of interest of the cryo-preserved specimen prior to X-ray microscopic investigations are highly desirable.

2.10. Imaging characteristics

The spectral resolution of the system is demonstrated by investigating the absorption spectrum of titanium-dioxide particles [see Figs. 4(*a*) and 4(*b*)]. As a comparison the spectrum of the same particles recorded at a scanning transmission X-ray microscope (STXM) equipped with a spherical-grating monochromator and dedicated for spectral analysis is shown. From these and other measurements the monochromaticity at XM-2 is 300 ($E/\Delta E$) when using a 20 µm pinhole. From our experience so far, after having collected many thousands of data sets, the characteristics of the condenser do not change over time. Objective lenses are replaced depending on the degradation of efficiency; in practice, this takes place every four to six months of operation (equates to the acquisition of approximately 480000 images). Using a photodiode chip (International Radiation Detectors AXUV-100; Funsten *et al.*, 2004) we estimate illuminating flux in the specimen region to be 5×10^7 photons s^{-1} μm^{-2} over a field of view of 15 µm × 15 µm.

The depth of field is comparable with the thickness of many mammalian cells, in which case the image formation process can be assumed to be well approximated parallel projections of the specimen's X-ray absorption. By taking images over a range of rotation angles, three-dimensional information of the specimen can be recovered using tomographic reconstruction methods. For most biological specimen tomographic data, this is essential because subcellular structures are confusingly superimposed in two-dimensional projection images.

2.11. Operation

Beamline 2.1 was designed, built and is now operated by staff of the National Center for X-ray Tomography (NCXT). The center was established to create a new modality for biomedical research and to address an unmet need for methods that can visualize minimally processed cells cryo-preserved in a near-native state. Potential users of this resource can apply for access *via* an independent peer review system managed by ALS staff (http://www-als.lbl.gov/index.php/holding/58-apply-for-beamtime.html). Cells suitable for imaging should be less than 15 µm thick and sufficiently robust that they can withstand being pipetted into a specimen capillary. Whilst the microscope field of view is 15 µm × 15 µm, cells larger than this in one dimension can be imaged easily by simply translating the specimen holder along the z-axis and collecting a series of tomographic data sets. Once the tomographic data sets are reconstructed they can easily be stitched together to generate a virtual field of view; for example, see the 50 µm hyphal yeast described previously (Uchida *et al.*, 2009) and the example shown in Fig. 5.

3. Ancillary facilities

The NCXT laboratories, located adjacent to XM-2, are fully equipped for cell biology research. Users have access to confocal microscopes and the capability to culture bacteria, fungi or eukaryotic cells (a listing of the available instruments can be found on-line, http://ncxt.lbl.gov). A feature unique to the NCXT is the availability of a high-numerical-aperture cryogenic light microscopy for correlated imaging studies (McDermott *et al.*, 2009; Le Gros *et al.*, 2009). This microscope has been enhanced by the incorporation of a cryogenic rotation stage to allow acquisition of cryogenic fluorescence tomography data (McDermott *et al.*, 2009, 2012; Smith *et al.*, 2013; Cinquin *et al.*, 2014).

3.1. Specimen handling and ancillary stages

We have two light microscopes in close proximity to the X-ray microscope for the purpose of pre-screening and investigating the specimen before X-ray imaging. One visible-light microscope is located next to the X-ray microscope to examine room-temperature test specimens frequently used to align the X-ray microscope and to characterize new zone-plate lenses. This microscope is an Olympus upright with a cooled CCD camera capable of performing fluorescence measurements. A second visible-light microscope, the alignment microscope, is mechanically connected to the X-ray microscope to allow viewing of the specimen once mounted on the X-ray microscope. This visible-light microscope operates in reflection mode. The microscope interfaces with the specimen cryo-stage to allow imaging of frozen specimens, an important feature in aligning the

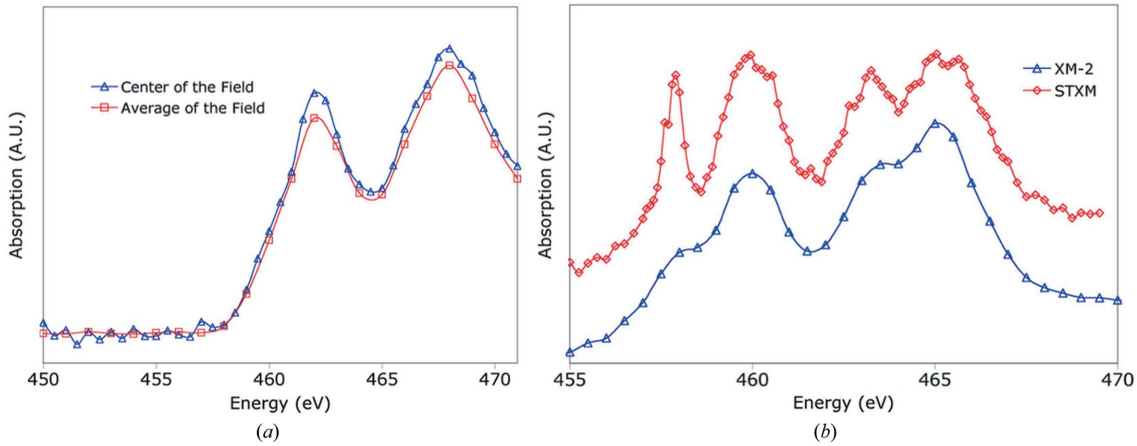

Figure 4
Spectral scan of titanium film. (*a*) The blue line shows the aborption spectrum taken with the condenser remaining stationary from the center of the field of view; the red line shows the absorption spectrum from the integral of the whole image with the condenser in 'scanning' mode to produce uniform illumination. (*b*) TiO_2 absorption spectral scan. Blue line from XM-2, red line from ALS beamline 5.3.2, a scanning transmission X-ray microscope (STXM).

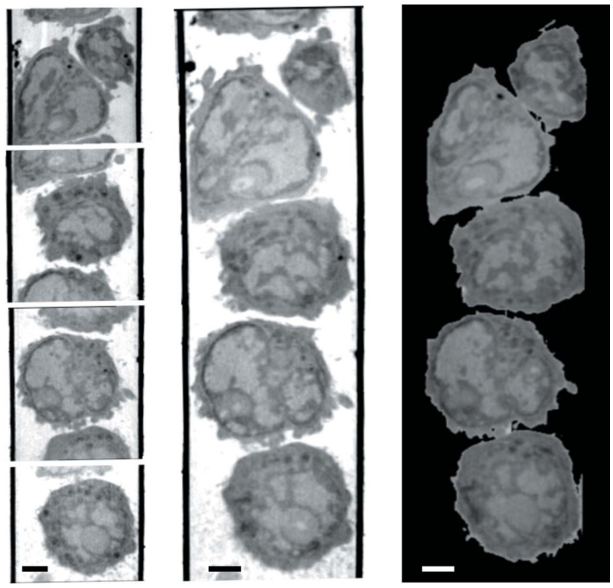

Figure 5
Soft X-ray tomography of mouse lymphocytes. (*a*) Slices through the tomographic reconstructions of four adjacent fields of view from the same capillary. (*b*) Same four fields of view shown in (*a*) after being aligned and computationally stitched together to form a single composite reconstruction. (*c*) Representative orthoslice through the cells shown in (*b*), after removing the glass capillary from view. Scale bars = 2 µm.

specimen in the X-ray microscope as well as in the initial axial centering of the tube tomography specimen.

3.2. Computational infrastructure and microscope control system

The NCXT computer system hardware is split between two locations, XM-2 on the ALS experimental floor and in a suite of laboratories in an adjacent building. A fully dedicated 10 GB high-bandwidth fiber channel connection facilitates rapid transfer of data between the two locations. Centralized network servers residing in the laboratory spaces provide authentication and storage for users on network workstations. The key services provided on our network are open directory for authentication and portable home directories, web service for electronic lab notebooks and information dissemination, and an image database that stores and collates experimental data. By using portable directories, staff and users are able to log in to any computer in our facility and see their home directory and workspace. Groups of users collaborating on projects have access to shared volumes that are only accessible by the appropriate user accounts. All of these data are routinely and automatically backed up using *Retrospect* to facilitate recovery and version control if necessary.

4. Recent highlight

XM-2 has now been used to image cells that range in scale and complexity from simple bacteria to complex eukaryotic cells. Recently the Lomvardas group from UCSF used XM-2 to answer a long-standing question regarding the epigenetic regulation of olfactory receptors (Clowney *et al.*, 2012). This work, some of which is shown in Fig. 6, is an elegant demonstration of the capabilities of XM-2 for imaging and quantifying sub-cellular structures.

5. Discussion and conclusions

Soft X-ray tomography is a highly informative method for visualizing and quantifying cells and sub-cellular structures. Cryo-preserved cells can be imaged with an isotropic spatial resolution of 50 nm, or better, without causing discernible radiation damage. Since SXT image contrast is generated by the differential absorption of photons, cells can be imaged without the use of potentially damaging contrast-enhancing procedures. XM-2 is used primarily for imaging cells that

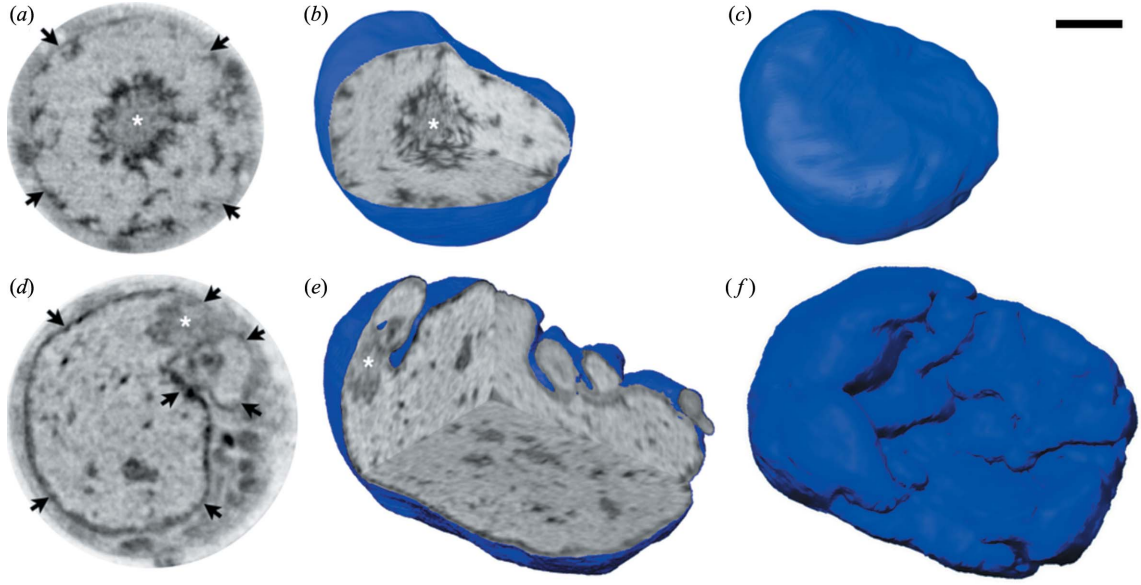

Figure 6
Soft X-ray tomography of mouse olfactory sensory neurons (OSNs). (*a*)–(*c*) Control OSN; (*d*)–(*f*) OSN expressing exogenous Lamin B receptor (LBR). (*a*, *d*) Orthoslices from the tomographic reconstructions; (*b*, *e*) three orthogonal orthoslices through the same nuclei shown in (*a*, *d*), respectively; (*c*, *f*) surface views of the same nuclei revealing the highly folded nuclear envelope in the enlarged nucleus expressing LBR (*f*). Asterisks show the mass of pericentromeric heterochromatin located in the center of the nucleus in control OSN (*a*, *b*) and displaced in the nucleus expressing LBR (*d*, *e*); arrows in (*a*, *d*) point to the nuclear periphery, which appears thicker in (*d*) after expression of LBR. Reproduced from Clowney *et al.* (2012). Scale bar = 2 µm.

undergo morphological changes during natural or induced processes. Some of these studies have included determining the consequences of exposing cells to candidate drug molecules, monitoring the etiology of diseases (such as viral infections), as well as the localization of molecules involved in these processes through the use of correlated cryogenic fluorescence tomography. Multi-modal light and soft X-ray imaging is beginning to make an impact in research areas as diverse as basic cell biology, biomedicine and biofuel development, and is poised to become a mainstream imaging approach in the future.

We thank Drs Dula Parkinson and Christian Knoechel for their assistance in the preparation of Fig. 4 and Dr David Kilcoyne for his expert help on ALS beamline 5.3.2. The Advanced Light Source is supported by the US Department of Energy, Office of Basic Energy Science (DE-AC02-05CH11231). The National Center for X-ray Tomography is supported by: the US Department of Energy, Office of Biological and Environmental Research (DE-AC02-05CH11231); the National Center for Research Resources of the National Institutes of Health (P41RR019664); the National Institute of General Medicine of the National Institutes of Health (P41GM103445). The Gordon and Betty Moore Foundation (3497) support our development of 'super resolution' cryo-fluorescence tomography for correlated imaging studies.

References

Attwood, D. T. (1999). *Soft X-rays and Extreme Ultraviolet Radiation: Principles and Applications.* Cambridge University Press.
Cardone, G., Grünewald, K. & Steven, A. C. (2005). *J. Struct. Biol.* **151**, 117–129.
Chao, W., Fischer, P., Tyliszczak, T., Rekawa, S., Anderson, E. & Naulleau, P. (2012). *Opt. Express*, **20**, 9777–9783.
Cinquin, B. P., Do, M., McDermott, G., Walters, A. D., Myllys, M., Smith, E. A., Cohen-Fix, O., Le Gros, M. A. & Larabell, C. A. (2014). *J. Cell. Biochem.* **115**, 209–216.
Clowney, E. J., LeGros, M. A., Mosley, C. P., Clowney, F. G., Markenskoff-Papadimitriou, E. C., Myllys, M., Barnea, G., Larabell, C. A. & Lomvardas, S. (2012). *Cell*, **151**, 724–737.
Falcone, R., Jacobsen, C., Kirz, J., Marchesini, S., Shapiro, D. & Spence, J. (2011). *Contemp. Phys.* **52**, 293–318.
Funsten, H. O., Ritzau, S. M., Harper, R. W. & Korde, R. (2004). *Appl. Phys. Lett.* **84**, 3552.
Hagen, C., Guttmann, P., Klupp, B., Werner, S., Rehbein, S., Mettenleiter, T. C., Schneider, G. & Grünewald, K. (2012). *J. Struct. Biol.* **177**, 193–201.
Hirai, A., Takemoto, K., Nishino, K., Niemann, B., Hettwer, M., Rudolph, D., Anderson, E., Attwood, D., Kern, D. P., Nakayama, Y. & Kihara, H. (1999). *Jpn. J. Appl. Phys.* **38**, 274–278.
Hummel, E., Guttmann, P., Werner, S., Tarek, B., Schneider, G., Kunz, M., Frangakis, A. S. & Westermann, B. (2012). *PLoS One*, **7**, e53293.
Kirz, J., Jacobsen, C. & Howells, M. (1995). *Q. Rev. Biophys.* **28**, 33–130.
Larabell, C. A. & Le Gros, M. A. (2004). *Mol. Biol. Cell*, **15**, 957–962.
Larabell, C. A. & Nugent, K. A. (2010). *Curr. Opin. Struct. Biol.* **20**, 623–631.
Le Gros, M. A., McDermott, G. & Larabell, C. A. (2005). *Curr. Opin. Struct. Biol.* **15**, 593–600.
Le Gros, M. A., McDermott, G., Uchida, M., Knoechel, C. G. & Larabell, C. A. (2009). *J. Microsc.* **235**, 1–8.
McDermott, G., Le Gros, M. A., Knoechel, C. G., Uchida, M. & Larabell, C. A. (2009). *Trends Cell Biol.* **19**, 587–595.
McDermott, G., Le Gros, M. A. & Larabell, C. A. (2012). *Annu. Rev. Phys. Chem.* **63**, 225–239.
Parkinson, D. Y., Epperly, L. R., McDermott, G., Le Gros, M. A., Boudreau, R. M. & Larabell, C. A. (2013). *Methods Mol. Biol.* **950**, 457–481.
Parkinson, D. Y., Knoechel, C., Yang, C., Larabell, C. A. & Le Gros, M. A. (2012). *J. Struct. Biol.* **177**, 259–266.
Rehbein, S., Guttmann, P., Werner, S. & Schneider, G. (2012). *Opt. Express*, **20**, 5830–5839.
Sakdinawat, A. & Attwood, D. (2010). *Nat. Photon.* **4**, 840–848.
Schneider, G., Guttmann, P., Heim, S., Rehbein, S., Mueller, F., Nagashima, K., Heymann, J. B., Müller, W. G. & McNally, J. G. (2010). *Nat. Methods*, **7**, 985–987.
Schneider, G., Guttmann, P., Rehbein, S., Werner, S. & Follath, R. (2012). *J. Struct. Biol.* **177**, 212–223.
Smith, E. A., Cinquin, B. P., McDermott, G., Le Gros, M. A., Parkinson, D. Y., Kim, H. T. & Larabell, C. A. (2013). *J. Struct. Biol.* **184**, 12–20.
Uchida, M., McDermott, G., Wetzler, M., Le Gros, M. A., Myllys, M., Knoechel, C., Barron, A. E. & Larabell, C. A. (2009). *Proc. Natl Acad. Sci. USA*, **106**, 19375–19380.
Vila-Comamala, J., Jefimovs, K., Raabe, J., Pilvi, T., Fink, R. H., Senoner, M., Maassdorf, A., Ritala, M. & David, C. (2009). *Ultramicroscopy*, **109**, 1360–1364.
Weiss, D., Schneider, G., Niemann, B., Guttmann, P., Rudolph, D. & Schmahl, G. (2000). *Ultramicroscopy*, **84**, 185–197.
Weiss, D., Schneider, G., Vogt, S., Guttmann, P., Niemann, B., Rudolph, D. & Schmahl, G. (2001). *Nucl. Instrum. Methods Phys. Res. A*, **467**, 1308–1311.